Electrochimica Acta 130 (2014) 29–39

Contents lists available at ScienceDirect

Electrochimica Acta

journal homepage: www.elsevier.com/locate/electacta

Electrochemical and Surface Characterization of Uranium Dioxide Containing Rare-Earth Oxide (Y_2O_3) and Metal (Pd) Particles

Mayuri Razdan[a], Martin Trummer[b], Dmitrij Zagidulin[a], Mats Jonsson[b], David W. Shoesmith[a,c,*]

[a] Department of Chemistry, Western University, London, Ontario, Canada N6A 5B7
[b] KTH Chemical Science and Engineering, Nuclear Chemistry, Royal Institute of Technology, SE-100 44 Stockholm, Sweden
[c] Surface Science Western, London, Ontario, Canada N6G 0J3

ARTICLE INFO

Article history:
Received 30 November 2013
Received in revised form 20 January 2014
Accepted 24 February 2014
Available online 11 March 2014

Keywords:
Uranium dioxide
Cyclic voltammetry
Raman spectroscopy
X-ray photoelectron spectroscopy
Dopants

ABSTRACT

Four specimens of uranium dioxide doped with rare-earth oxide (Y_2O_3) and/or metal particles (Pd) i.e., UO_2, UO_2-Y_2O_3, UO_2-Y_2O_3-Pd, UO_2-Pd were surface and electrochemically characterized using scanning electron microscopy (SEM/EDX), Raman spectroscopy, X-ray photoelectron spectroscopy (XPS) and cyclic voltammetry. Surface analyses showed that the dopants are present as a separate phase in the UO_2 matrix and all oxides are non-stoichiometric and contain a large number of defect clusters. Voltammetry shows anodic oxidation begins at sub-thermodynamic potentials and the presence of multiple cathodic reduction peaks indicates the presence of a number of structural domains with different electrochemical reactivities. Corrosion potential (E_{CORR}) and polarization resistance measurements (Rp) in the presence of H_2O_2 suggests that the anodic reactivity of all the specimens is comparable and high compared to 1.5 at% SIMFUEL. The lower Rp values obtained on the doped specimens is consistent with the presence of readily oxidizable cuboctahedral clusters in the oxide matrix.

1. Introduction

A considerable effort is underway in the nuclear industry to minimize the potential impact of hazardous radioactive spent-fuel on the environment. Proposed solutions range from reprocessing to direct disposal in a deep geologically-stable repository. A multi-barrier approach to radionuclide containment is internationally universal and comprises the fuel waste form itself, a metal container, a clay buffer compacted around the container, repository sealing materials, and the geologic formation [1–3].

The spent-fuel has a very low solubility in the reducing groundwaters expected to prevail at a repository depth of ≥ 500 m. However, radioactive decay processes within the fuel will cause water radiolysis to produce reactive species (H_2O_2, $HO^{\bullet}$ etc) [1] and generate oxidizing conditions at the UO_2 surface. Consequently, H_2O_2, expected to be the primary radiolytic oxidant, could promote corrosion of the UO_2 [4], especially when the UO_2^{2+} complexing agent, HCO_3^-/CO_3^{2-}, is present in the groundwater [5–8].

While the establishment of oxidizing conditions provides the primary driving force, the corrosion performance of the fuel will also be influenced by the fission products produced in the fuel matrix during in-reactor burnup. The composition of fission products is determined by the initial enrichment of the fuel and its in-reactor irradiation history. The typical burn-up range for CANDU fuel is 120 to 320 MWh/kgU [3] but is significantly higher for LWR/PWR fuel [9,10]. Consequently, used nuclear fuel will consist of ~95% UO_2, with the remaining 5% being radioactive fission products and transuranium elements present in various chemical states. Depending on in-reactor history these fission products redistribute within the fuel. Volatile species (Xe, Kr, I) can diffuse out of the fuel matrix to the fuel cladding gap while other elements precipitate in metallic (Mo, Ru, Pd, Ru) and oxide form (Rb, Cs, Ba, Zr) or remain in solid solution (transuranium and rare earth elements (REE)) in the UO_2 matrix [9].

A number of physical and chemical changes induced by in-reactor irradiation would be expected to change the reactivity of the fuel [11]. These include primarily, (a) the introduction of grain boundary tunnels; (b) the generation of trapped fission gas bubbles; (c) the generation of noble metal particles; (d) the rare-earth doping of the UO_2 matrix; and (e) the presence of non-stoichiometry. In this paper we are primarily interested in the chemical changes

* Corresponding author. Tel.: +1 631 344 76 4; fax: +1519 661 2111x86366.
E-mail address: dwshoesm@uwo.ca (D.W. Shoesmith).

http://dx.doi.org/10.1016/j.electacta.2014.02.134
0013-4686/

(c) to (e) which can be simulated in custom-fabricated UO_2/UO_{2+x} specimens.

The influence of rare-earth dopants, which occupy lattice sites in the fuel matrix, on air oxidation of UO_2 has been well studied (M = Gd, Y, La [12–17]). This reaction proceeds in two stages,

$$UO_2 \rightarrow U_3O_7/U_4O_9 \rightarrow U_3O_8 \quad (1)$$

via a U_3O_7 intermediate for pure UO_2 whereas, when the UO_2 is substantially doped, the intermediate is U_4O_9. The second step involving the recrystallization to U_3O_8 is kinetically hindered by rare earth doping [12,17,18] as indicated by the increase in temperature required to force the recrystallization to occur. Based on this evidence for air oxidation, a similar influence of rare earth doping on corrosion might be anticipated since the reaction proceeds by a similar two stage sequence,

$$UO_2 \rightarrow UO_{2+x} \rightarrow UO_2^{2+} \quad (2)$$

except the final product is dissolved UO_2^{2+} as opposed to a recrystallized deposit of U_3O_8.

Some support for this expectation is evident in electrochemical experiments on SIMFUELs in which a decrease in anodic dissolution current was observed as the extent of simulated burn up increased. SIMFUELs are natural stoichiometric UO_2 pellets doped with 11 non-radioactive elements (Ba, Ce, La, Mo, Sr, Y, Zr, Rh, Pd, Ru, Nd) to replicate the chemical effects of in-reactor irradiation [10,11]. The amount of the individual elements added simulates a specific degree on in-reactor burnup. The key features of these simulated fuels are the rare earth doping of the UO_2 matrix and the presence of noble metal (Rh, Pd, Ru) particles. The observed decrease in anodic current was attributed to the influence of the rare earth dopants in solid solution in the UO_2 matrix.

Non-stoichiometry has also been shown to exert a significant influence on UO_2 reactivity [11]. MicroRaman spectroscopy showed very distinct changes in fuel structure as x (in UO_{2+x}) increases. Studies using AFM, current-sensing AFM and scanning electrochemical microscopy [19] demonstrated that the fuel reactivity increased substantially with highly non-stoichiometric UO_{2+x} being $\geq 10^3$ more reactive than close to stoichiometric UO_{2+x}. While the exact mechanistic details remain unresolved, the extent of oxidation on a surface close to stoichiometric appears limited by the low interstitial mobility within the matrix. At higher degrees of non-stochiometry the formation of defect clusters enhances O interstitial mobility [11].

In this paper our primary interest is in the influence of rare-earths and noble metals contained within the UO_2 matrix. Recent studies [20] showed that the addition of small amounts of Y_2O_3 (0.3 wt%) to UO_2 decreased the corrosion rate (compared to UO_2) by a factor of 3 to 5. Since the rate of H_2O_2 consumption was very similar for UO_2 and UO_2/Y_2O_3, this decrease was attributed to a decrease in reactivity of the UO_2/Y_2O_3 pellet. However, the degree of non-stoichiometry of these pellets was not characterized.

To further investigate the influences of rare earth doping and the presence of noble metal particles we have performed a series of electrochemical and corrosion experiments on UO_2 and UO_2/Y_2O_3 pellets with and without added Pd. The electrodes were characterized by scanning electron microscopy (SEM), energy dispersive X-ray analysis (EDX), Raman spectroscopy and X-ray photoelectron spectroscopy (XPS). The redox behavior was characterized by cyclic voltammetry (CV) and the anodic reactivity by potentiostatic oxidation. Corrosion behavior was investigated in H_2O_2–containing solutions purged with Ar.

2. Experimental

2.1. Fuel specimens and electrode preparation

Four different electrodes were used in this study consisting of undoped UO_2 and UO_2 doped with Y_2O_3 (0.3 wt%) and/or Pd (1 wt%) received from The Royal Institute of Technology, Stockholm, Sweden. These electrodes were fabricated using depleted UO_2 powder, Y_2O_3 powder (particle size $\sim$ 5 μm) and Pd powder (particle size $\sim$ 1.0–1.5 μm) as described by Trummer et al. [20,21]. The electrodes were prepared from the pellets using a previously published methodology [22] and are designated UO_2, UO_2-Pd, UO_2-Y_2O_3, and UO_2-Y_2O_3-Pd. Prior to electrochemical experiments and surface analyses electrodes were polished (wet) with a 1200 grit polishing paper and rinsed with deionized water.

2.2. Solutions

All solutions were prepared with analytical grade chemicals and distilled deionized water (ρ =18.2 MΩ cm) prepared using a Millipore Milli-Q-plus unit to remove organic and inorganic impurities. Experiments were performed in a 0.1 mol.L^{-1} NaCl solution (Caledon, >99%) purged with Ar (Praxair). Prior to the start of any experiment solutions were purged with Ar gas for a minimum of 1 hr. When borate buffered solution was used, 0.05 mol.L^{-1} borax (Merck) was added to the solution prior to the pH adjustment. The solution pH was adjusted to the desired value using NaOH and was monitored with an Orion model 720A pH meter and adjusted accordingly. Solutions containing H_2O_2 (Fisher Scientific, 3%) were prepared by dilution. The concentration of H_2O_2 was determined using a BioLogic Science Instruments MOS UV/VIS spectrophotometer [23].

2.3. Electrochemical measurements

All experiments were carried out in a standard three-electrode, three-compartment cell. The WE was attached to the shaft of a Pine Instruments model AFASR analytical rotator to allow electrode rotation when required. The counter electrode was a Pt sheet (~6 cm^2) spot-welded to a Pt wire. All electrochemical experiments were performed (22 ± 2 °C) using a Solartron model 1287 potentiostat to control applied potentials and record current responses. The current interrupt method was employed to eliminate the potential (iR) drop caused by the ohmic resistance (R) primarily in the electrode. Corrware™, version 3.0, software was used to analyze the data. All the potential measurements reported are quoted on the saturated calomel electrode (SCE) scale.

2.4. Experimental procedure

Before all experiments the electrode was cathodically reduced at two different potentials (usually -1.5 V and -1.2 V) for 2 to 5 minutes, the H_2 gas bubbles produced at the more negative potential being released while still maintaining cathodic control at the less negative potential. In CV experiments, the potential was scanned from the starting potential to different anodic limits and back while recording the current.

In potentiostatic experiments the potential was pulsed to +0.4 V after cathodic cleaning and the current measured over a period of 30 min at an electrode rotation rate of 16.67 Hz in Ar-purged solution. The electrode was rotated to ensure that the reaction was interfacially controlled. In corrosion experiments the E_{CORR} was followed in a 0.1 mol.L^{-1} NaCl + 0.01 mol.L^{-1} $NaHCO_3$ (pH $\sim$ 9.0) solution purged with Ar until a steady-state value was achieved. Hydrogen peroxide was then added and the E_{CORR} measurement continued. A series of linear polarization resistance (LPR)

measurements was made before and after H_2O_2 addition. In LPR measurements a small potential, in the range of ±10 mV with respect to E_{CORR} is applied at a scan rate of 0.0167 mV/sec and the resulting (linear) current response measured. The LPR (Rp) is the ratio of the applied potential to the current response and is inversely proportional to the uniform charge transfer rate at the electrode/solution interface. Electrochemical experiments were repeated twice to assure the reproducibility of the results.

2.5. Surface analysis

2.5.1. Scanning electron microscopy (SEM)/Energy dispersive X-ray (EDX) analyses

An Hitachi S-4500 Field emission scanning electron microscope (SEM) coupled with a Quartz XOne energy dispersive X-ray (EDX) system was used for imaging. The SEM micrographs were obtained on polished electrodes with the varied electron beam potential ranging from 10.0 kV to 15.0 kV. EDX mapping was performed to obtain the size, distribution and elemental composition of the doping elements in the host matrix. The chemical composition of individual particles was also determined.

2.5.2. Raman spectroscopy

Raman spectra were acquired on all four electrodes using a Renishaw 2000 confocal Raman spectrometer (Renishaw PLC., UK). Raman active vibrations were excited using a HeNe laser with a wavelength of 632.8 nm which produces ~ 2 μm diameter focused beam at the sample surface. The laser was used at 50% power to avoid laser heating since small changes in temperature can produce small changes in the frequency and width of Raman lines. The spectrometer was calibrated using a Si crystal standard at room temperature. The laser beam was focused onto the sample mounted on a Leica DMLM microscope with a 50x uncoated objective lens. Each spectrum was measured for an exposure time of ~45 sec over the wavenumber range 120 to 1400 cm^{-1}. Measurements were repeated at a number of different locations on the electrode to ensure uniformity of response. The Lorentzian peak model and a Shirley baseline correction were used to fit the Raman peaks.

2.5.3. X-ray photoelectron spectroscopy(XPS)

XPS analyses were performed on a Kratos Axis NOVA spectrometer. Spectra were collected using Al K_α -monochromatic radiation (15 mA, 14 kV) to bombard the surface with high energy monochromatic X-rays ($h\nu$ = 1486.6 eV). The instrument work function was set to give a binding energy (BE) of 83.96 eV for the Au $4f_{7/2}$ line for metallic Au and the spectrometer dispersion was adjusted to give a BE of 932.62 eV for the Cu $2p_{3/2}$ line of metallic Cu. Survey spectra were recorded over the energy range 0 to 1100 eV on an analysis area of ~300 × 700 μm at a pass energy of 160 eV. High resolution spectra for the U 4f, O 1s, C 1s and the U 5f valence band

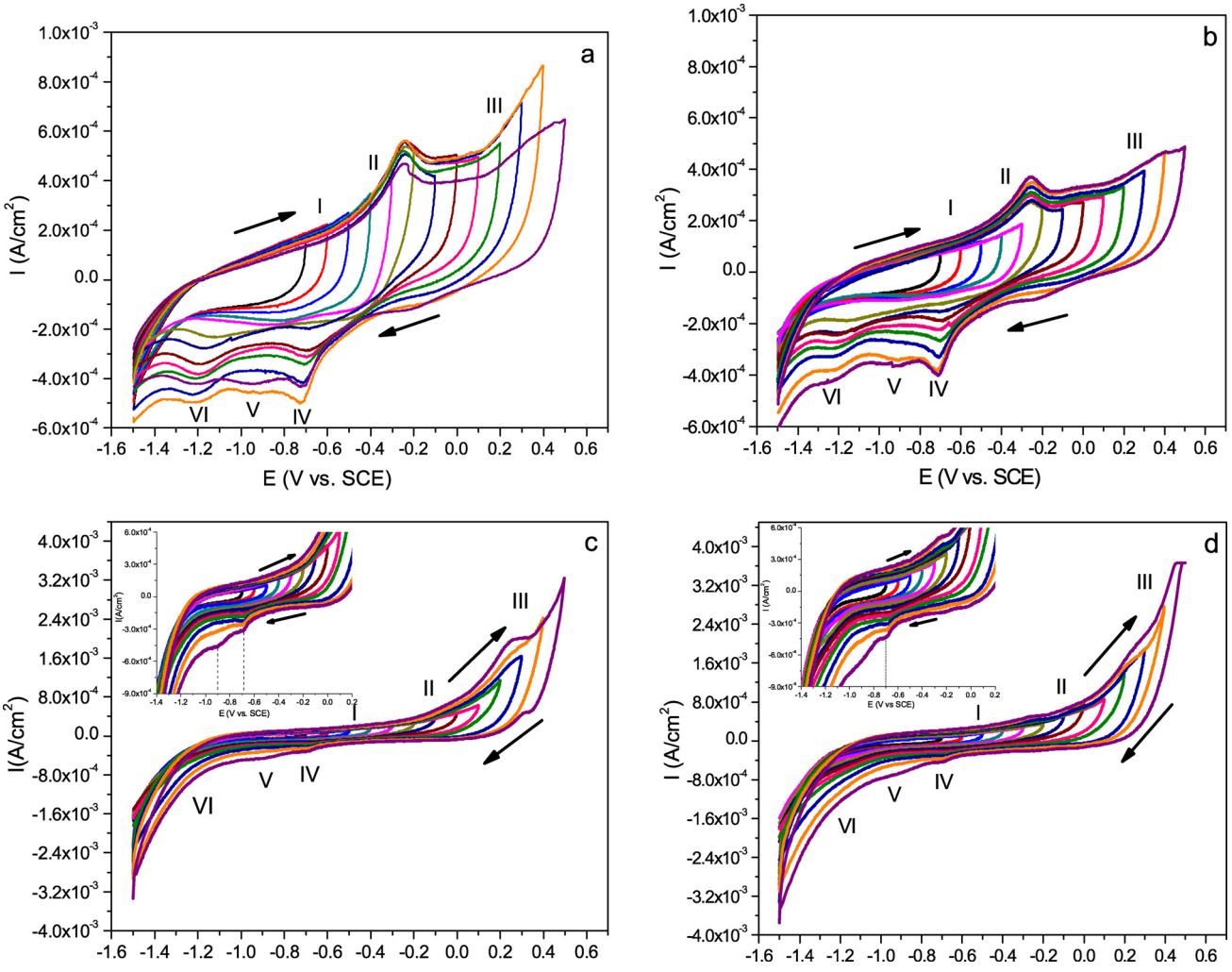

Fig. 1. CV's to various anodic limiting potentials recorded on the (a) UO_2 (b) UO_2-Y_2O_3 (c) UO_2-Y_2O_3-Pd (d) UO_2-Pd electrodes in Ar-purged 0.1 mol.L^{-1} NaCl solution buffered with sodium borate (0.05 mol.L^{-1}) at pH~9 (22 ± 2 °C). The scan rate = 5 mV.s^{-1}.

regions were collected with a pass energy of 20 eV. The instrument charge neutralizer was used on all specimens. The carbon 1s line at 285 eV was used as a standard, when necessary, to correct for surface charging. Spectra were analysed using CasaXPS software (version 2.3.14). The 4f spectrum was deconvoluted into contributions from U^{IV}, U^{V} and U^{VI} by fitting both the two spin-orbit split peaks and the associated satellite structures following the procedure described elsewhere [23]. Surface analysis was conducted on unpolished (as-received) and polished electrodes in order to ensure the reproducibility of surface characteristic.

3. Results

3.1. Voltammetric behavior

Fig. 1 (a to d) shows a series of IR-compensated CVs recorded on the four electrodes to different anodic potential limits. Several stages of oxidation and reduction are observed and the profiles for UO_2 and UO_2-Y_2O_3 ((a) and (b)) are effectively identical. On the two electrodes which contain Pd (UO_2-Pd and UO_2-Y_2O_3-Pd; (c) and (d)) the same stages of oxidation and reduction appear to be present but are swamped by the very large currents observed at the positive and negative potential limits of the scan.

According to previous electrochemical and XPS studies performed on UO_2 and SIMFUEL (1.5 at% simulated burn-up; i.e., only lightly doped), oxidation of a stoichiometric surface should not be observed until the applied potential is > –0.4 V [1,22]. However, on the electrodes used in this study, a shallow oxidation is observed over the potential range -0.8 V to -0.4 V (I in Fig. 1), leading to an equally shallow reduction process over the potential range -0.6 V to -1.2 V. A current at such low potentials was previously attributed to the oxidation of hyperstoichiometric UO_{2+x} locations on the UO_2 surface [1]. More recently, this "sub-thermodynamic" oxidation was shown to be a feature of non-stoichiometric UO_{2+x} [24].

Over the potential range -0.4 V to -0.1 V a distinct anodic oxidation peak is observed (II in Fig. 1) leading to an equally distinct cathodic reduction peak at ~ -1.2 V (VI in Fig. 1). A similar oxidation-reduction couple was observed previously on a uranium dioxide specimen with an average stoichiometry of $UO_{2.011}$ and known to possess distinct regions with various stoichiometries [25]. Anodic oxidation leading to a reduction process requiring such a negative potential is indicative of the formation of a very stable oxidized state. The nature of this state is presently obscure although it is clearly associated with the oxidation of already non-stoichiometric locations.

When the anodic limit is extended to potentials ≥ -0.2 V the oxidation current is sustained and leads to the development of a cathodic reduction peak at ~ -0.7 V (IV in Fig. 1). Oxidation and reduction in these potential ranges has been convincingly attributed to the oxidation of stoichiometric UO_2 and the subsequent reduction of the UO_{2+x}/UO_3.yH_2O formed [1,24,26]. For potentials positive to ~ 0.2 V the current increases further (III in Fig. 1) leading to an increase in the reduction peaks at both -1.2 V and -0.7 V consistent with the more extensive oxidation of both non-stoichiometric and stoichiometric locations on the UO_2 surface. In addition, a new reduction peak develops in the potential range -0.9 to -1.0 V (V in Fig. 1). A similar oxidation peak was observed previously [25] and tentatively attributed to the anodic oxidation of deeper locations in an already oxidized surface layer. The potential required to reduce this oxidized state is considerably more negative (~ -0.9 V) than that required to reduce the film formed on stoichiometric UO_2 (-0.7 V) consistent with the claim by He [25] that the reduction of deeply oxidized states is involved. Previously, the reduction peaks at -0.9 V and -1.2 V have only been seen after the anodic oxidation of a non-stoichiometric $UO_{2.011}$ electrode [25] clearly indicating that the UO_2 and UO_2-Y_2O_3 electrodes are non-stoichiometric or a mixture of non-stoichiometric and stoichiometric regions.

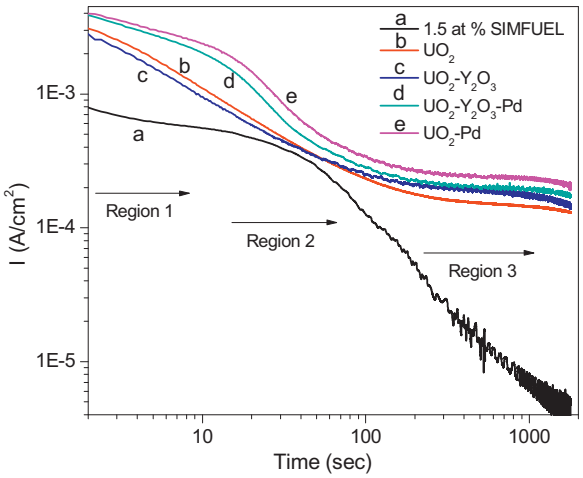

Fig. 2. Potentiostatic current-time curves recorded on a 1.5 at% SIMFUEL, and the four electrodes at +0.4 V for 30 min in Ar purged 0.1 mol.L^{-1} NaCl buffered with sodium borate (0.025 mol.L^{-1}) at pH~ 9 (22 ± 2 °C).

The same general features are observed on the UO_2-Pd and UO_2-Y_2O_3-Pd electrodes but are more difficult to see due to the large positive and negative currents, most likely due to water oxidation (to O_2) and reduction (to H_2) on the Pd particles in the electrodes. These results demonstrate, (i) the influence of the Pd content on the anodic current and (ii) the marginal influence of the Y-content on the anodic behaviour of the UO_{2+x}.

Fig. 2 shows a series of such experiments conducted at a potential of 0.4 V for 30 minutes at an electrode rotation rate of 16.7 Hz with the current density (I) plotted logarithmically as a function of the log of time. This potential was chosen since all the possible electrochemical reactions feasible on the UO_2 surface will be occurring and the current response will reflect the overall anodic reactivity. A more extensive investigation of the individual anodic reactions is being undertaken and will be published separately. An experiment on 1.5 at% SIMFUEL is included for comparison since this electrode has been well studied previously [22,26].

As shown, the SIMFUEL behavior is very different to that observed on the other four electrodes. The current at short times is considerably lower and the decrease in current at longer times consistent with previous electrochemical and XPS experiments which showed anodic oxidation proceeded through the sequence

$$UO_2 \rightarrow UO_{2+x} \rightarrow UO_3.yH_2O \quad (3)$$

with the formation of the U^{VI} oxide layer leading to a general passivation of the surface [27]. The other four electrodes all exhibited considerably higher currents at short times and especially at longer times. The increased currents at short times indicate a significant increase in overall reactivity of the electrodes compared to the stoichiometric, but rare earth doped SIMFUEL. Also, at short times, the currents observed on the two Pd-containing electrodes are slightly higher than on the other two electrodes as observed at this potential under voltammetric conditions (Fig. 1). However, this difference is temporary and disappears for times ≥ 30s. As noted when discussing the CV behavior it is likely that this enhanced current can be attributed to H_2O oxidation on Pd particles (see below). At longer times all four electrodes exhibit almost identical behavior and approach steady-state with no tendency to passivate. Such behavior has only previously been observed on non-stoichiometric electrodes which have been shown to exhibit enhanced anodic reactivity [25].

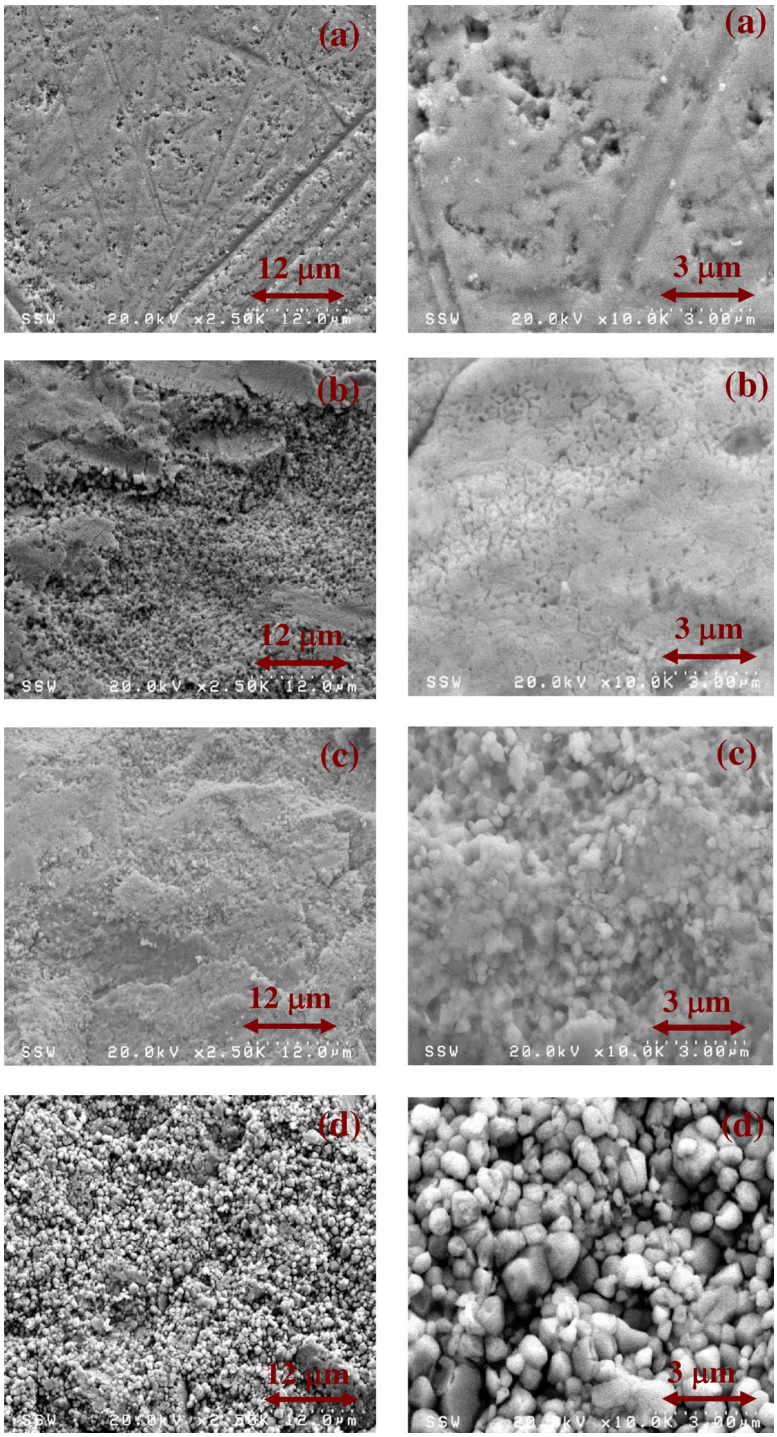

Fig. 3. SEM micrographs recorded on the (a) UO_2 (b) UO_2-Y_2O_3 (c) UO_2-Y_2O_3-Pd and (d) UO_2-Pd electrodes.

3.2. Surface characterization

3.2.1. SEM/EDX analysis

Fig. 3 shows SEM images of the surfaces of the four electrodes. At the higher magnification the surfaces appear rough and finely particulate. Figs. 4 and 5 show SEM images and EDX maps recorded on the UO_2-Y_2O_3 and UO_2-Y_2O_3-Pd electrodes and show that both the Y and Pd are unevenly distributed in the host matrix and present as individual particles of different sizes and shapes. This is expected for Pd which has a very low solubility in the UO_2 matrix. The Pd particles formed are significantly larger than the particle size of the Pd powder (1-1.5 μm), used in their fabrication, which has been attributed to the compaction technique used when forming the pellets [20]. Similarly distributed Pd particles were observed in the UO_2-Pd electrode (not shown).

These maps show that the majority, perhaps all, of the Y is present in particulate form as a separate phase and not incoRporated in solid solution in the UO_{2+x} matrix. This is consistent with the voltammetric data, Figs. 1 and 2, which show no significant influence of Y on the electrochemical behavior of the pellets.

3.2.2. Raman analysis

Fig. 6 shows the Raman spectra recorded on all four electrodes. Raman scattering for stoichiometric UO_2 should generate a

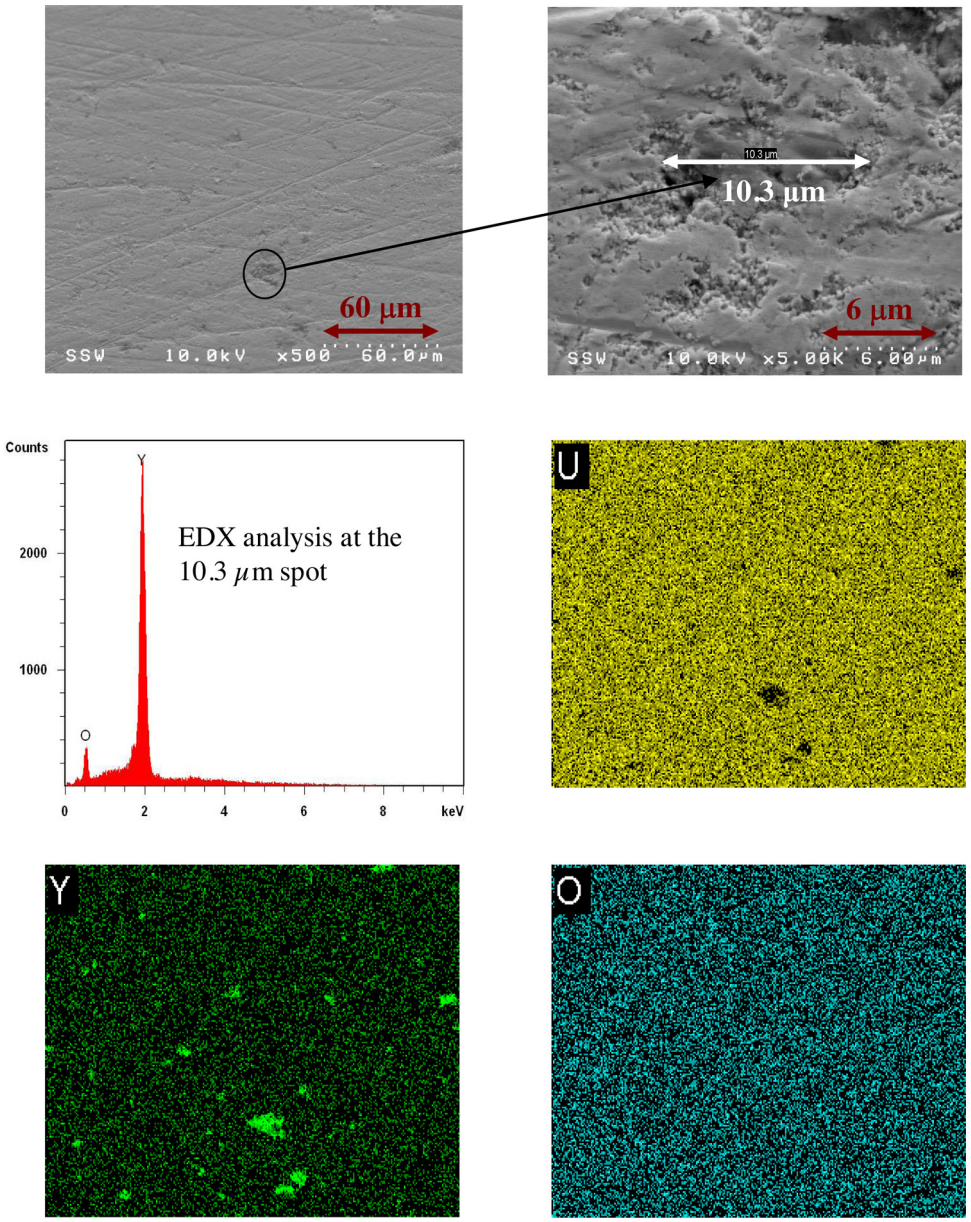

Fig. 4. SEM micrographs recorded on a UO_2-Y_2O_3 electrode and the corresponding EDX maps for U, Y and O. An EDX spectrum recorded on the identified particle is also shown.

fundamental vibrational stretch at ~ 450 cm^{-1} and a second band at ~ 1150 cm^{-1} [28–30]. The 450 cm^{-1} (T_{2g}) stretch is ascribed to the symmetric (g) stretching mode due to O breathing vibrations around U^{IV} in the fluorite structure of UO_2, whereas the ~ 1150 cm^{-1} band can be assigned to an overtone of the first order LO phonon at 575 cm^{-1}. The 1150 cm^{-1} band has been shown to be highly sensitive to the extent of non-stoichiometry of the UO_2 [31].

Inspection of the spectra showed the T_{2g} band is broad and shifted to higher frequency (445 to 455 cm^{-1}) for all four electrodes. Desgranges et al. [32] attributed this shift to the local disorder involved in U_4O_9 formation, U_4O_9 being a UO_2 based lattice containing clusters of interstitial O atoms (cuboctahedra) and U in higher oxidation states. Deconvolution of this band is shown for the UO_2-Y_2O_3 electrode in Fig. 7 yields peaks at 455 and 475 cm^{-1}, the 475 cm^{-1} peak suggesting a distortion of the cubic symmetry induced by the increasing concentration of O excess defects [31]. However, a similar Raman shift to higher frequency and the development of asymmetry was reported as a consequence of rare-earth (Sm^{III}) doping in TiO_2 samples [33], and other authors attributed a peak at ~ 480 cm^{-1} to the Raman active E_g (U-O) stretching mode, a characteristic of the tri-uranium octaoxide (α-U_3O_8) [29,34,35]. Although not shown an identical deconvolution is obtained on the other three electrodes.

In addition to this shift in the T_{2g} band, all four spectra exhibit a broad band between 500 and 700 cm^{-1} commonly attributed to O sublattice damage [27,28,32,36], Fig. 6. The intensity of this band is significantly greater than that of the T_{2g} band, a feature previously shown to be associated with a high degree of non-stoichiometry ($0.25 \leq x \leq 0.33$) [31]. As shown in Fig. 7 for the UO_2-Y_2O_3 electrode this broad band can be deconvoluted into peaks at 585 cm^{-1} and 630 cm^{-1}. The peak at 585 cm^{-1} is not generally associated with stoichiometric UO_2 and has been attributed to the presence of bulk defects [37]. It is also possible it is associated with the peak commonly observed at 575 cm^{-1}, a forbidden first order LO Raman scattering mode allowed as a consequence of the breakdown in selection rules due to disorder induced by the presence of defects.

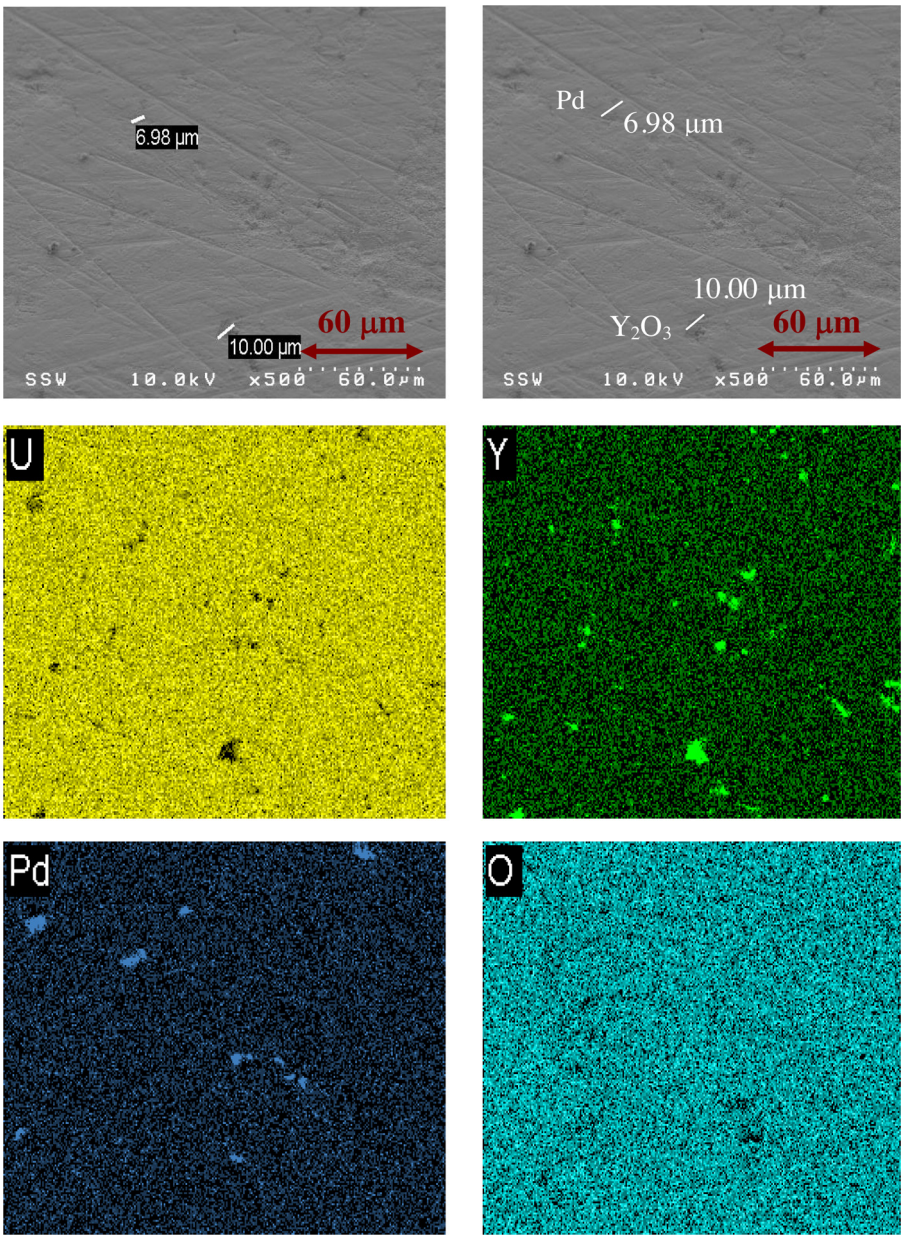

Fig. 5. SEM micrographs recorded on the UO_2-Y_2O_3-Pd electrode and the corresponding EDX maps for U, Y, Pd and O.

Such a breakdown would be expected from a loss of translational symmetry at vacancy sites due to O defect clustering and the change in cation radius when U^{IV} is converted to U^{V} with increasing non-stoichiometry. Again, although not shown, an identical deconvolution was obtained for the spectra recorded on the other three electrodes.

The strong peak at 630 cm^{-1} (an A_{1g} stretch) has been frequently observed on hyperstoichiometric UO_{2+x} and on rare earth doped SIMFUELs [31,32,38,39]. Its universal observance in the spectra recorded on all four electrodes indicates it is most appropriately assigned to hyperstoichiometry in the present case. Original suggestions that this band in UO_{2+x} could be attributed to distortion of the anion sublattice due to the O ion displacements required to accommodate excess O ions were recently confirmed by Desgranges et al. [32] who demonstrated this peak was a signature of the cuboctahedral cluster associated with the presence of U_4O_9. The small peak at 155 to 160 cm^{-1} is similarly associated with U_4O_9 [32] and attributed to the distortion of the cation sublattice associated with the formation of a tetragonal structure. A similar band has been reported for tetragonal zirconia (ZrO_2) [40].

3.2.3. XPS analysis

Fig. 8(i) shows a deconvoluted high resolution XPS spectrum recorded on the freshly polished UO_2-Y_2O_3 electrode. Identical spectra were observed (but are not shown) for the other electrodes. The location of the satellite peak at a binding energy of ~7 eV higher than the U $4f_{5/2}$ peak confirms that U^{IV} is the dominant oxidation state present in the electrode surface. There is also a measurable U^{V} content indicated by the presence of the satellite peak at a binding energy ~ 8 eV above the U $4f_{5/2}$ peak. The relative amounts of U^{IV} and U^{V} are only marginally influenced by the presence of Y and Pd, Fig. 8(ii). This is especially true for U^{V}. Noticeable amounts of U^{VI} were also detected, possibly due to air-oxidation while transferring the specimens from the polishing area to the vacuum chamber of the XPS spectrometer. These observations, and the very high U^{V} content, confirm the

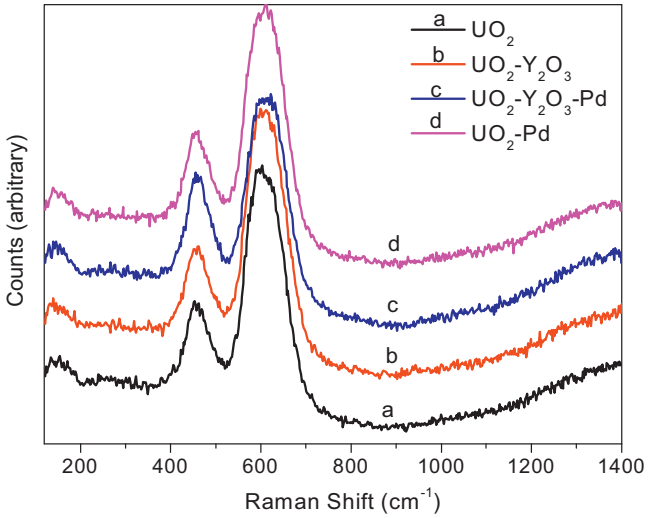

Fig. 6. Raman spectra recorded on the four polished electrodes.

specimens are non-stoichiometric in agreement with the Raman and electrochemical results. It is worth noting that XPS analyses on SIMFUELs showed the U^V content increased from ~17% to ~26% as the extent of simulated burnup (and hence the rare earth doping level of the UO_2 matrix) increased from 1.5 at% to 6.0 at%. This can be compared to the 36 to 37% measured on these four electrodes.

3.3. *Corrosion potential (E_{CORR}) and linear polarization resistance (Rp) measurements in H_2O_2 solutions*

Corrosion experiments were conducted on rotating electrodes (16.7 Hz) in an Ar-purged 0.1 mol.L^{-1} NaCl solution containing 0.01 mol.L^{-1} $NaHCO_3$ (pH ~ 9.0). The corrosion potential, E_{CORR}, was monitored on each electrode until steady-state was achieved and then 2 mmol.L^{-1} H_2O_2 was added to the cell and the E_{CORR} measurement continued, Fig. 9. Prior to H_2O_2 addition, E_{CORR} reaches a steady-state value almost immediately on the SIMFUEL electrode but this required a few hours on the other four electrodes. Eventually, E_{CORR} for the SIMFUEL achieves a value ~ 70 mV more negative than the values recorded on the other four electrodes.

Series of LPR measurements were conducted at regular intervals and the Rp values are plotted in Fig. 10. The first two data points

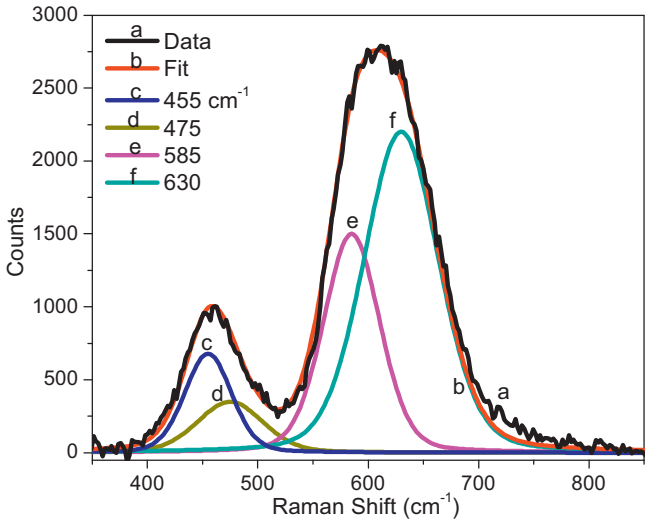

Fig. 7. Fitted and deconvoluted Raman bands for the wavenumber range 350 cm^{-1} to 850 cm^{-1} on UO_2-Y_2O_3 electrode.

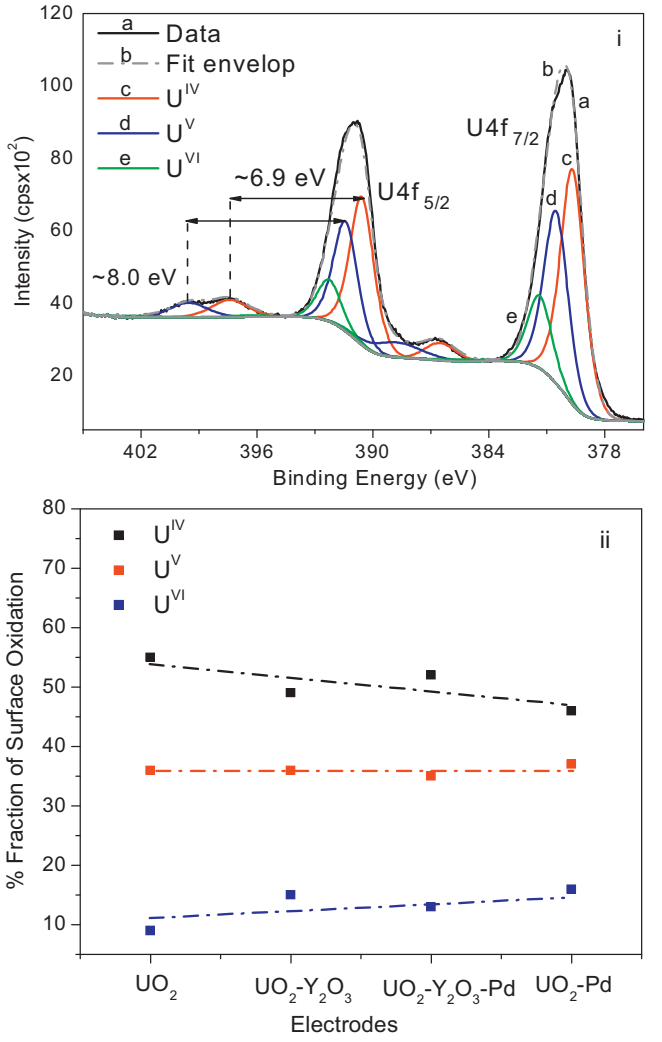

Fig. 8. (i) Fitted and deconvoluted XPS spectra for the U-4f region recorded on UO_2-Y_2O_3 electrode; (ii) Relative fractions of all three oxidation states obtained from the XPS curve fitting.

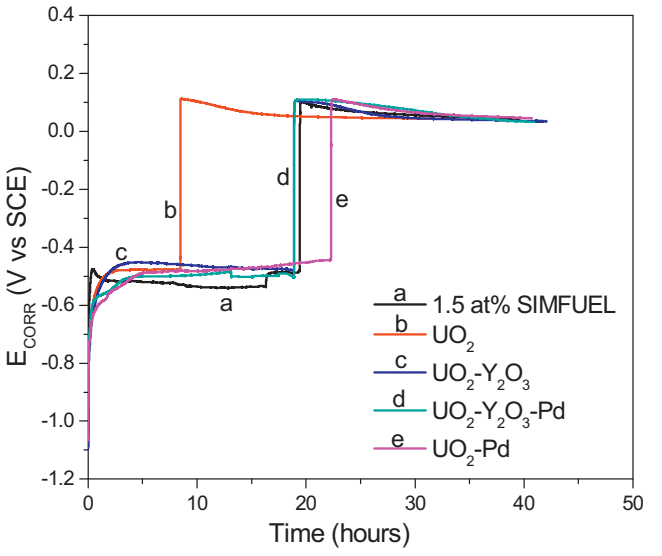

Fig. 9. E_{CORR} recorded as a function of time before and after the addition of H_2O_2 (2 mmol.L^{-1}) to an Ar -purged 0.1 mol.L^{-1} NaCl solution containing 0.01 mol.L^{-1} $NaHCO_3$ at pH ~9.0 (22 ± 2 °C): the sudden increases in E_{CORR} occur immediately on H_2O_2 addition.

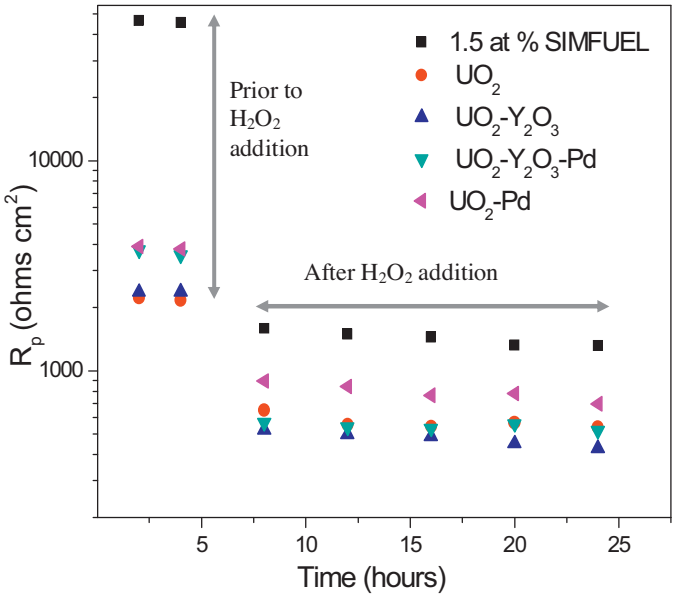

Fig. 10. Polarization resistance (Rp) values recorded at various times before and after the addition of 2 mmol.L^{-1} of H_2O_2 to an Ar-purged 0.1 mol.L^{-1} NaCl solution containing 0.01 mol.L^{-1} $NaHCO_3$ at pH ~9.0 (22 ± 2 °C). The Rp values are normalized to ejected time which is four hours prior to H_2O_2 addition.

for each electrode are Rp values recorded prior to H_2O_2 addition and the subsequent five data points show the values recorded with H_2O_2 present. Once the H_2O_2 was added the solution composition was identical to that used by Trummer et al. [20,41] in experiments on these electrodes in which H_2O_2 consumption and U dissolution rates were measured.

Except for SIMFUEL no significant influence of electrode composition on E_{CORR} is observed. This difference in E_{CORR} leads to differences in Rp, the value for SIMFUEL being over an order of magnitude greater than the values on the other electrodes. The Rp values on the two Pd-containing electrodes are ~ 30% higher than on the two Pd-free electrodes.

After H_2O_2 addition, E_{CORR} increases immediately to a steady-state value of 100 mV on all five electrodes. This shift is accompanied by a decrease in Rp values consistent with a reactivity of H_2O_2 on the electrode surfaces. While the Rp value on SIMFUEL remains larger than that on the other four electrodes the difference is reduced to only a factor of 2 to 4. For the four non-stoichiometric electrodes the difference in Rp values remains small but the value on the UO_2-Pd electrode is noticeably different than on the other three electrodes. The values are effectively constant with time on all the electrodes. Subsequent inspection of the electrodes by SEM (not shown) shows no visible change in the state of the surfaces, indicating that no significant corrosion damage occurred over the duration of these experiments.

4. Discussion

SEM/EDX, Raman spectroscopy and XPS have been used to characterize UO_2 electrodes containing Y and Pd. SEM/EDX showed the electrodes were rough and finely particulate with Y and Pd generally distributed throughout the matrix as Y_2O_3 and Pd particles.

All four materials (UO_2, UO_2-Y_2O_3, UO_2-Pd, UO_2-Y_2O_3-Pd) exhibited very similar Raman and XPS spectra. The dominance of the Raman peak in the wavelength number range 500 to 700 cm^{-1} and the absence of the LO phonon overtone at 1150 cm^{-1} indicate the oxide is non-stoichiometric. According to Manara and Renker [29], the 1150 cm^{-1} peak disappears as the stoichiometry approaches $UO_{2.1}$ but more recent studies indicate that the O in non-stoichiometric UO_{2+x} may not be homogeneously distributed [25]. Evidence that the latter is the case with the materials in this study comes from deconvolution of the Raman peak in the 500 to 700 cm^{-1} region which yields peaks at 585 cm^{-1} and 630 cm^{-1}. The dominance of the latter peak confirms that the oxide contains a large number of cuboctahedral U_4O_9 clusters. In addition small bands at 475 cm^{-1} and 155 cm^{-1} indicate a distortion of the U sublattice consistent with the onset of the transformation to U_3O_7. These features show that, at least some areas within the oxide are highly non-stoichiometric.

The XPS results confirm that this non-stoichiometry is reflected in the surface composition. The deconvoluted U4f peaks show that all the specimens exhibited a U^V content in the range 36 to 37% compared to 17 to 26% for rare earth doped SIMFUELs (over the simulated burn up range from 1.5 at% to 6.0 at%).

The electrochemical behavior is also consistent with specimens containing a mixture of stoichiometric and non-stoichiometric domains. In voltammetric experiments the presence of a current at sub-thermodynamic potentials is attributed to the facile oxidation of non-stoichiometric domains. The composition of the oxidized product is unknown but the need for a very negative potential to cause its reduction confirms that it is very stable. The oxidation and reduction processes expected for stoichiometric UO_2 are also observed. From voltammetric experiments alone it is not possible to determine either the degree of non-stoichiometry or the distribution of stoichiometric and non-stoichiometric material.

An anodic oxidation experiment comparing the electrochemical reactivity of these specimens to that of the well characterized 1.5 at% SIMFUEL showed them to be very reactive. Unlike on SIMFUEL, the anodic current did not decrease substantially with time as expected for the formation of a passivating U^{VI} surface layer. Instead the four specimens behaved identically (at times > 40s) in establishing a long-term steady-state oxidation current. Although this anodic reactivity has not been investigated in detail the anodic product must be either a deeply oxidized, but non-passivating, surface layer or the enhanced dissolution of U^{VI} (as UO_2^{2+}). Since the pH was borate buffered at pH ~ 9.0 in these experiments extensive dissolution is not anticipated.

The reciprocal of Rp (Rp^{-1}) is directly proportional to the rate of charge transfer at the electrode/solution interface and for a corroding system would be proportional to the corrosion rate. Prior to the addition of H_2O_2 the corrosion experiments show there is a significant difference between the Rp values measured on SIMFUEL and those measured on the other four electrodes despite the effectively identical E_{CORR} values. In the absence of a specific oxidant in the solution this difference most likely reflects charge transfer processes within the surface of the UO_{2+x}. For stoichiometric SIMFUEL previous studies show no discernible reactivity at potentials in the vicinity of the measured E_{CORR} (~ -0.5 V) at which the Rp measurements were made. For the other electrodes the CVs in Fig. 1 show that charge transfer processes occur on non-stoichiometric locations, and this could account for the much lower Rp values recorded.

After the addition of H_2O_2 two charge transfer processes are possible: (i) corrosion of the UO_{2+x} (UO_2) leading to the formation of soluble UO_2^{2+}; while dissolution would be expected to dominate over the formation of a U^{VI} deposit in the carbonate solution used, the deep oxidation of the non-stoichiometric surface is also likely [25]; (ii) H_2O_2 decomposition to O_2 and H_2O. This last reaction could occur on the UO_2 (UO_{2+x}) surface, Y_2O_3 particles, and especially on Pd particles.

In the absence of additional analytical information, a linear polarization measurement cannot distinguish between these two reactions, and the Rp value will reflect some composite value of

the resistance to both processes. In comparison to the analytical results of Trummer et al. [20] and Pehrman et al. [41] the Rp value will be comparable to the total H_2O_2 consumption rate by both the corrosion and decomposition reactions.

The values in Fig. 10 show Rp for the SIMFUEL is noticeably greater than the values for the other electrodes when H_2O_2 is present, and with the exception of the UO_2-Pd specimen the other values are effectively indistinguishable. Analytical experiments on SIMFUEL [41] show that while the rate of H_2O_2 consumption is similar to that observed on the UO_2 and UO_2-Y_2O_3 electrodes, the U dissolution rate (which is a measure of the corrosion rate) is negligible. Although the doping level (expressed as a simulated burnup) of the SIMFUEL used is not given it will contain noble metal particles which would support the decomposition process. However, a considerable amount of electrochemical evidence exists [7,42] showing that the H_2O_2 is reactive on the UO_2 surface and that, at the E_{CORR} achieved ($\sim +0.1$ V) the system is redox buffered by the H_2O_2 decomposition reaction. The results of Pehrman et al. [41] indicate that the rare earth doped stoichiometric UO_2 matrix in the fuel is very stable under these conditions.

The similarity in Rp values for the UO_2 and UO_2-Y_2O_3 electrodes is consistent with the observations of Trummer et al. [20] who showed that the H_2O_2 consumption and U dissolution rates were only slightly lower on the UO_2-Y_2O_3 pellet than on the UO_2 pellet, the Y_2O_3 particles exerting little influence on the H_2O_2 consumption rate. Since the Y is not distributed within the uranium oxide matrix the similarity in Rp values (surface reactivities) can be attributed to the identical nature of the oxide matrices as demonstrated voltammetrically and by Raman spectroscopy. The lower Rp values on the UO_2 and UO_2-Y_2O_3 electrodes compared to the SIMFUEL can be predominantly attributed to the destabilizing influence of cuboctahedral clusters in the matrix and their ability to support reactions involving H_2O_2.

5. Summary and Conclusions

The electrochemical and corrosion behavior of a series of uranium dioxide electrodes containing Y_2O_3 and Pd have been characterized by Raman spectroscopy and XPS and their reactivity investigated electrochemically. Both the Y_2O_3 and the Pd were shown to be present in particulate form and the uranium dioxide matrix was shown to contain both stoichiometric and non-stoichiometric domains.

Raman spectroscopy showed the oxides contained a high content of cuboctahedral clusters and voltammetry suggested that these domains within the fuel are oxidized at sub-thermodynamic potentials.

Electrochemical experiments showed that the anodic oxidation of these domains was extensive and not limited by the formation of a passive U(VI) layer, as observed for SIMFUEL.

Corrosion potential and linear polarization resistance measurements confirmed the electrodes were more electrochemically reactive than SIMFUEL in H_2O_2-containing solutions. As suggested by the electrochemical results all the electrodes exhibited very similar corrosion behavior in H_2O_2 solutions.

The results confirm that the degree of non-stoichiometry will be a dominant influence in determining the reactivity of spent fuel under permanent waste disposal conditions. Although extensive non-stochiometry is not expected in spent fuel its existence in grain boundaries within the fuel matrix is possible potentially making these locations more susceptible to corrosion than the stoichiometric grains. Presently, it is assumed that the fission product inventory at these locations would be rapidly released on contact of the fuel with groundwater. Until a more comprehensive understanding of the influences of rare earth doping and non-stoichiometry in fuel corrosion is available this conservative assumption should be retained.

Acknowledgements

This research is funded under the Industrial Research Chair agreement between the Canadian Natural Sciences and Engineering Research Council (NSERC) and Nuclear Waste Management Organization (NWMO), Toronto, Canada. The Swedish Nuclear Fuel and Waste Management Company (SKB) is also acknowledged for financial support. Surface Science Western is greatly acknowledged for the use of their XPS, Raman and SEM equipment.

References

[1] D.W. Shoemsith, Journal of Nuclear Materials 282 (2000) 1.
[2] Nuclear Waste Management Organization (NWMO), Choosing a Way Forward: the Future Management of Canada's Used Nuclear Fuel, November 2005, http://www.nwmo.ca
[3] J. McMurry, D. A. Dixon, J. D. Garroni, B. M. Ikeda, S. Stroes-Gascoyne, P., Baumgartner, T. W. Melnyk, Ontario Power Generation Report No: 06819-REP-01200-10092-R00, 2003.
[4] K. Ollila, Posiva Oy: 2011-27, Eurajoki, Finland, May 2011.
[5] I. Grenthe, J. Fuger, R.J. Konings, R.J. Lemire, A.B. Muller, C. Nguyen-Trung, H. Wanne, Chemical Thermodynamics of Uranium, North Holland, Amsterdam, 1992.
[6] D. W. Shoesmith, S., Sunder, W. H. Hocking, Electrochemistry of Novel Materials, ed. J. Liplowski and P. N. Ross, Vol. 297, New York, 1994.
[7] J.S. Goldik, J.J. Noël, D.W. Shoesmith, Electrochimica Acta 51 (2006) 3278.
[8] S. Rollin, K. Spahiu, U.B. Eklund, Journal of Nuclear Materials 297 (2001) 231.
[9] H. Kleykamp, Journal of Nuclear Materials 131 (1985) 221.
[10] L. H. Johnson and D. W. Shoesmith, In Radioactive Waste Forms for the Future, ed. W. Lutze and R. Ewing, Amsterdam, 1988.
[11] H. He, M. Broczkowski, K. O'Neil, D. Ofori, O. Semenikhin, D.W. Shoesmith, Nuclear Waste Management Organization, Ontario, Toronto, 2012.
[12] J-Goo Kim, Y-Keong Ha, S-Dal Park, K-Yong Jee, W-Ho Kim, Journal of Nuclear Materials 297 (2001) 327.
[13] W.B. Wilson, Journal of Inorganic and Nuclear Chemistry 20 (1961) 242.
[14] L.E. Thomas, R.E. Einziger, H.C. Buchanan, Journal of Nuclear Materials 201 (1993) 310.
[15] G.S. You, K.S. Kim, D.K. Min, S.G. Ro, Journal of Nuclear Materials 277 (2000) 325.
[16] R.D. Scheele, D.B. Hanson, E.S. Cumblidge, D.E. Jenson, E.A. Kozelisky, L.R. Sell, J.P. MacFarlan, L.A. Snow, Material Research Society Symposium Proceedings 824 (2004) 211.
[17] R.J. McEachern, D.C. Doern, D.D. Wood, Journal of Nuclear Materials 252 (1998) 145.
[18] J-Won Choi, R.J. McEachern, P. Taylor, D.D. Wood, Journal of Nuclear Materials 230 (1996) 250.
[19] H. He, Z. Qin, D.W. Shoesmith, Electrochimica Acta 56 (2010) 53.
[20] M. Trummer, B. Dahlgren, M. Jonsson, Journal of Nuclear Materials 407 (2010) 195.
[21] M. Trummer, S. Nilsson, M. Jonsson, Journal of Nuclear Materials 378 (2008) 55.
[22] B.G. Santos, H.W. Nesbitt, J.J. Noel, D.W. Shoesmith, Electrochimica Acta 49 (2004) 1863.
[23] M. Razdan, D.S. Hall, P.G. Keech, D.W. Shoesmith, Electrochimica Acta 83 (2012) 410.
[24] H. He, R.K. Zhu, Z. Qin, P. Keech, Z. Ding, D.W. Shoesmith, Journal of the Electrochemical Society 156 (2009) C87.
[25] H. He, Ph.D. Thesis, Department of Chemistry, University of Western Ontario, London, Canada, 2010.
[26] B.G. Santos, J.J. Noël, D.W. Shoesmith, Journal of Electroanalytical Chemistry 586 (2006) 1.
[27] D. Ofori, MS Thesis, University of Western Ontario, London, Canada, 2008.
[28] H. He, P.G. Keech, M.E. Broczkowski, J.J. Noel, D.W. Shoesmith, Canadian Journal of Chemistry 85 (2007) 1.
[29] D. Manara, B. Renker, Journal of Nuclear Materials 321 (2003) 233.
[30] S.D. Senanayake, G.I.N. Waterhouse, A.S.Y. Chan, T.E. Madey, D.R. Mullins, H. Idriss, Catalysis Today 120 (2007) 151.
[31] H. He, D. Shoesmith, Physical Chemistry Chemical Physics 12 (2010) 8108.
[32] L. Desgranges, G. Baldinozzi, P. Simon, G. Guimbretière, A. Canizares, Journal of Raman Spectroscopy 43 (2012) 455.
[33] C.H. Yang, Z.Q. Ma, Applied Optics 51 (2012) 5438.
[34] S.D. Senanayake, R. Rousseau, D. Colegrave, H. Idriss, Journal of Nuclear Materials 342 (2005) 179.
[35] C. Jégou, R. Caraballo, S. Peuget, D. Roudil, L. Desgranges, M. Magnin, Journal of Nuclear Materials 405 (2010) 235.

[36] J.R. McBride, K.C. Hass, B.D. Poindexter, W.H. Weber, Journal of Applied Physics 76 (1994) 2435.
[37] H. Idriss, Surface Science Reports 65 (2010) 67.
[38] E.A. Stefaniak, A. Alsecz, I.E. Sajó, A. Worobiec, Z. Máthé, S. Török, R.V. Grieken, Journal of Nuclear Materials 381 (2008) 278.
[39] A. Seibert, S. Stumpf, D. Schild, T. Gouder, D. Bosbach, Institute for Transuranium Elements FZKA 7489, Karlsruhe, Germany, 2009.
[40] P. Bouvier, G. Lucazeau, Journal of Physics and Chemistry of Solids 61 (2000) 569.
[41] R. Pehrman, M. Trummer, C.M. Lousada, M. Jonsson, Journal of Nuclear Materials 430 (2012) 6.
[42] S. Sunder, N.H. Miller, D.W. Shoesmith, Corrosion Science 46 (2004) 1095.